

Effects of Fiber Orientation on the Frictional Properties and Damage of Regenerative Articular Cartilage Surfaces

Mario Alberto Accardi, PhD,¹ Seth D. McCullen, PhD,²⁻⁴ Anthony Callanan, PhD,²⁻⁴
Sangwon Chung, PhD,²⁻⁴ Philippa M. Cann, PhD,¹ Molly M. Stevens, PhD,^{2-4,*} and Daniele Dini, PhD^{1,*}

Articular cartilage provides a low-friction, wear-resistant surface for diarthrodial joints. Due to overloading and overuse, articular cartilage is known to undergo significant wear and degeneration potentially resulting in osteoarthritis (OA). Regenerative medicine strategies offer a promising solution for the treatment of articular cartilage defects and potentially localized early OA. Such strategies rely on the development of materials to restore some aspects of cartilage. In this study, microfibrinous poly(ϵ -caprolactone) scaffolds of varying fiber orientations (random and aligned) were cultured with bovine chondrocytes for 4 weeks *in vitro*, and the mechanical and frictional properties were evaluated. Mechanical properties were quantified using unconfined compression and tensile testing techniques. Frictional properties were investigated at physiological compressive strains occurring in native articular cartilage. Scaffolds were sheared along the fiber direction, perpendicular to the fiber direction and in random orientation. The evolution of damage as a result of shear was evaluated via white light interferometry and scanning electron microscopy. As expected, the fiber orientation strongly affected the tensile properties as well as the compressive modulus of the scaffolds. Fiber orientation did not significantly affect the equilibrium frictional coefficient, but it was, however, a key factor in dictating the evolution of surface damage on the surface. Scaffolds shear tested perpendicular to the fiber orientation displayed the highest surface damage. Our results suggest that the fiber orientation of the scaffold implanted in the joint could strongly affect its resistance to damage due to shear. Scaffold fiber orientation should thus be carefully considered when using microfibrinous scaffolds.

Introduction

ARTICULAR CARTILAGE is a resilient tissue covering the articulating surfaces of diarthrodial joints and exhibits remarkable friction and wear properties allowing the joint to function for a lifetime of movement.¹ However, etiologies, such as osteoarthritis (OA), trauma, aging, and developmental disorders, can result in degeneration or even loss of hyaline cartilage.² Clinical strategies for damaged articular cartilage and OA involve regenerative techniques, including microfracture, autologous chondrocyte implantation (ACI), and matrix-induced autologous chondrocyte implantation (MACI).³⁻⁶ MACI has significantly improved the traditional ACI technique by utilizing a range of commercially available fiber-based membranes, which are able to enhance cellular attachment, distribution, while eliminating several complications (periosteal flap harvest and implantation) and generating more predictable cell-material interactions.^{4,7-9} Current articular cartilage tissue grafts not only undergo

extensive loading regimens as neocartilage is formed, but also must provide a near frictionless surface. Thus, a key parameter of tissue scaffolds for articular cartilage is their bio-tribological performance. In this regard, reconstitution of the frictional properties of articular cartilage requires scaffolding with optimal design with regard to the microstructure, extracellular matrix (ECM) deposition/organization, as well as binding of appropriate molecules.¹⁰⁻¹²

Recent advances in scaffold materials have examined how the microstructure, as well as the chemical composition, can influence chondrocyte growth, distribution, matrix production, and the resulting biomechanical properties.¹³⁻¹⁵ However, few studies have investigated the frictional response of tissue-engineered articular cartilage.^{10,16-19} Thus, this research has focused on the functionality of such tissue grafts with particular interest in their frictional response. Fibrous scaffolds offer advantages in controlling the fiber size, spacing, and orientation.^{11,12} Control of fiber orientation is known to dictate differences in bulk tensile and compressive

¹Tribology Group, Department of Mechanical Engineering, Imperial College London, London, United Kingdom.

²Department of Materials, ³Department of Bioengineering, and ⁴Institute of Biomedical Engineering, Imperial College London, London, United Kingdom.

*These authors are co-corresponding authors.

properties and offers morphological similarities to articular cartilage.²⁰ For example, the superficial zone of naturally functioning articular cartilage consists of primarily flattened ellipsoidal-like chondrocytes and a very polarized dense organization of nanoscale collagen type II fibrils oriented parallel to the plane of the articular surface.²¹ The superficial zone consists of the highest concentration of collagen and the lowest concentration of proteoglycans. Based on the alignment of chondrocytes and collagen type II fibrils, the thin superficial zone has the greatest tensile strength found in articular cartilage, which is crucial for resisting shear and tensile forces from the articulating surfaces. Although electrospun scaffolds^{22,23} have been investigated for fibrous and hyaline cartilage replacement, the role of fiber orientation in such constructs has yet to be investigated as articular cartilage exhibits organization in both depth-dependent and surface directions.²⁴ Fiber alignment in the bulk scaffolds contributes significantly to the tensile properties, yet little is known regarding their frictional and wear performance.²⁵ Assessing the tribological performance and the evolution of damage in the scaffold is crucial as it will have to sustain complex loading in the joint before the formation of significant amounts of ECM. Herein, we assess the effect of fiber orientation in electrospun scaffolds on the friction and wear properties during cartilage regeneration. Our results demonstrate that, in addition to other mechanical properties, fiber orientation plays a critical role in the shear properties and, more specifically, damage during shear testing.

Materials and Methods

Scaffold fabrication and characterization

Poly(ϵ -caprolactone) (PCL) ($M_n = 80$ kDa) fibrous scaffolds were fabricated on a custom-made electrospinning device as described in our earlier work.¹⁵ The PCL solution (12 wt% in hexa-fluoro-isopropanol) was electrospun through a 19-gauge blunt tip needle at a flow rate of 2 mL/h, at 15 kV, with a spinneret-to-collector distance of 10 cm, and collected onto a rotating mandrel (width = 6 cm; diameter = 20 cm) at a linear velocity of either 1 or 15 m/s to form either randomly oriented or aligned fiber scaffolds, respectively.^{26,27} These electrospinning conditions were established after determining the optimal conditions through design of experiment analysis for electrospinning fibrous materials with a consistent fiber diameter of 1 μ m and varied fiber orientation of random isotropic fibrous scaffolds or aligned anisotropic fibrous scaffolds. The concentration of 12 wt% PCL (M_n : 80 kDa) in HFIP led to optimal molecular chain entanglements for fiber formation to occur without deformities in regard to beading or fiber irregularities. HFIP was chosen as the optimal solvent system based on its slow evaporation rate and high-solubility parameter. The operation settings of 15 kV, 10 cm, and 2 mL/h were based on ensuring proper Taylor cone formation to yield consistent fiber diameters. The collector was rotated at either 1 or 15 m/s to yield isotropic or anisotropic fiber networks. About 15 m/s was determined to align fiber scaffolds by moving at a velocity in the range of the velocity of the fiber jet moving from the Taylor cone to the rotating collector. The fiber size was optimized to be ~ 1 μ m and the fiber orientation was determined using small-angle light scattering as previously reported.²⁸ All scaffolds were ~ 1 mm in thickness, with an

average pore size of ~ 12 μ m and 80% porosity (determined by mercury porosimetry). Before chondrocyte seeding, 10-mm-diameter scaffolds were punched from macroscopic electrospun sheets and fiber orientation was conserved by cutting a small notch for identification in the outer diameter of all scaffolds. Tensile samples were cut from macroscopic sheets with a width of 10 mm and length of 50 mm.

Scaffolds were imaged using a JEOL 5610 (Herts) environmental scanning electron microscope. Specimens were coated with 100 \AA Au using an Emitech K550 sputter coater and observed at an accelerating voltage of 15 kV and a working distance of 10 cm.

Bovine chondrocyte, cell isolation, and scaffold interaction

Bovine chondrocyte isolation. Bovine cartilage was harvested from the lower leg joint of young calves and chondrocytes were isolated as previously described in our earlier work.¹⁵ Scaffolds were sterilized in 70% ethanol for 30 min followed by three washes with sterile phosphate-buffered saline (PBS), and then soaked in 0.01% v/v bovine serum albumin (Sigma) in PBS overnight to assist with chondrocyte adhesion.²⁰ Twenty microliters of an expansion medium containing 0.5 million bovine chondrocytes (passage 1) was placed on one side of each scaffold and cells were allowed to adhere for 2 h before seeding the other side with an additional 0.5 million chondrocytes. Following chondrocyte adhesion, fibrous scaffolds were transferred to nonadherent 24-well plates and cultured in 1 mL of the chondrogenic differentiation medium consisting of DMEM (4.5 g/L L-glucose), supplemented with 50 μ g/mL L-proline (Sigma), 50 μ g/mL ascorbic acid (Sigma), 0.1 mM sodium pyruvate (Sigma), 10 ng/mL TGF- β 3 (Lonza), and 1% v/v ITS Premix (BD Biosciences) at 37°C and 5% CO₂. The medium was changed twice weekly for 4 weeks *in vitro*.

Chondrocyte-scaffold interaction. Chondrocyte morphology on electrospun scaffolds was assessed by examining cytoskeletal organization by immunostaining. Scaffolds were fixed in 4% w/v paraformaldehyde for 15 min, washed twice with PBS, and permeabilized with 0.25% v/v Triton X-100 in PBS for 15 min. Actin cytoskeleton was stained with Alexa Fluor[®] 568 phalloidin (Invitrogen; 1:160) for 20 min and nuclei were stained with DAPI (Sigma; 1:1000) for 2 min. Type I and type II collagen were detected using the collagen I antibody (rabbit polyclonal, Ab34710) and collagen II antibody (dilution ratio 1:100, rabbit polyclonal, Ab34712; Abcam). Both antibodies were detected using the goat polyclonal secondary antibody to rabbit IgG with a FITC conjugation (Ab97050) (dilution ratio 1:1000) and counterstained with DAPI (Sigma; 1:1000) for 2 min. Sections were stained separately for collagens. Chondrocytes were imaged on an Olympus IX51 epifluorescence microscope equipped with an Olympus DP70 camera.

After 0 and 4 weeks of culture, chondrocyte-seeded scaffolds were digested in the papain solution (2.5 units papain/mL, 5 mM cysteine HCl, 5 mM EDTA, in PBS (all reagents from Sigma) at 60°C overnight. Digested samples were assayed for total DNA content using the Quant-iT[™] PicoGreen[®] kit (Invitrogen) according to the manufacturer's instructions. Sulfated glycosaminoglycan (sGAG) contents

were determined using the Blyscan Kit (Biocolor) as per the manufacturer's instructions.

Mechanical characterization, compressive and tensile properties

Compressive properties. After 0 and 4 weeks in culture, chondrocyte-seeded scaffolds were assessed for compressive properties by performing unconfined uniaxial compression testing using an Instron Model 5540 testing machine equipped with a 50N load cell. Three-millimeter-diameter samples were cored from 10-mm-diameter samples, preloaded to 0.05N,²⁰ allowed to equilibrate for 5 min, and then compressed to 10% strain at a crosshead speed of 0.5% strain/min, as previously reported.¹⁵ The tangent modulus was calculated from the linear portion of the stress-strain curve.

Stress relaxation tests on the samples were also performed to investigate any form of interstitial fluid support. Three-millimeter-diameter samples were cored from 10-mm-diameter samples preloaded to 0.05N, and then compressed to a low strain of 2% strain to examine the contribution of ECM deposition on the scaffolds and a high strain 18% ± 2.5% equivalent to the compressive load of 3N used in the shear tests. Indeed, a low strain means that most of the mechanical response would be given by the ECM, which is highly strained as compared to the scaffold. This allowed us to investigate the level of interstitial fluid support of the ECM avoiding potential masking effects from the compression of the scaffold itself. The crosshead speed was at 0.5% strain/min and samples were then allowed to relax for a period of 5 min under the high or low strain condition. Percentage relaxation was calculated at 1 and 5 min during the relaxation period.

Tensile properties. The response of the scaffolds under tensile loading was mechanically tested using the same machine used for compression testing, operated at a crosshead speed of 10 mm/min. Specimens had a gauge length of 30 mm, width of 10 mm, and thickness of 1 mm. The tensile modulus was calculated from the linear portion of the stress-strain curve after all specimens were tested to failure.

Fiber orientation effect on the frictional properties

Shear testing. Shear tests were performed using an in-house built Multi-axial Compression and Shear Testing Rig (MCSTR) specifically designed to test articular cartilage using a variety of physiological pressures, testing conditions, and configurations. Shear tests were carried out at constant load using a steel plate with $R_a \sim 1 \mu\text{m}$ as the counter interface. The rig is designed so that the steel counter surface is fixed, while the lower specimen was able to move both vertically (compression) and horizontally (sliding). For the scaffolds to be viable for shear testing, whole, 10-mm-diameter scaffolds were affixed onto high-density polyethylene (PE) discs using a thin layer of cyanoacrylate glue. Cellular and acellular (control) scaffolds were press fitted into the sample holder so that the PE disc was laterally constrained, raising the scaffold above the sample holder's height. Unless specified, in this study, throughout the text and the relevant figures and tables, acellular scaffolds refer to scaffolds with no cell-deposited ECM and no chondrocytes. Cellular scaffolds refer to

chondrocyte-seeded scaffolds after the full 4 weeks of culture time. Specimens were immersed in PBS at room temperature and equilibrated for 30 min before shear testing. Scaffolds were tested in shear using a 500 μm stroke length and a frequency of 2 Hz corresponding to a sliding speed of 2 mm/s. This sliding speed ensures boundary lubrication and is similar to previous studies on tissue-engineered articular cartilage tribology.^{17,19} To verify that the scaffolds were undergoing shear, force-displacement loops were produced confirming that shear was indeed taking place. Before testing, both deterministic and homogenized models, developed by Scaraggi and coworkers²⁹⁻³¹ for the study of lubricated soft rough contacts, were utilized to simulate the scaffold-steel platen interactions during sliding and to verify that the lubrication regime of the experimental test occurring during sliding was indeed boundary lubrication. The shear test parameters were input into the model as well as the mechanical properties of the scaffold (assumed to be elastic) and the measured topography of a representative sample's surface. Testing the scaffolds in the boundary regime was deemed as the most appropriate shear test condition to use, when evaluating the frictional response and surface damage, hence avoiding and potential masking effects, which could arise in fluid film lubrication.³²

Scaffold specimens were tested at loads of 3N and 6N corresponding to contact pressures of ~ 0.04 and 0.08 MPa, respectively. Testing was carried out on random and aligned scaffolds (sliding parallel and perpendicular to the fiber direction). Articular cartilage samples were also tested; cartilage plugs ($\phi 10$ mm) were extracted using a surgical coring device from healthy adult bovine knee joints, as previously reported.³² The native articular cartilage was used as a reference for assessing the frictional response of tissue-engineered articular cartilage.

Evaluation of surface properties and damage. Surface morphology was measured using white light interferometry (WLI) and scanning electron microscopy (SEM). Measurements were performed on the scaffolds before and after testing to quantify and visualize changes in surface topography as a result of shearing. WLI used a Wyko, NT9100 interferometric microscope, with a 20 \times magnification objective.³²⁻³⁴ Following shear testing, the samples were blotted to remove excess liquid and then imaged. WLI was used to obtain images of 312 \times 234 μm^2 and surface parameters. The surface parameter used in this study to assess roughness was R_a (mean surface roughness), which is a measure of the arithmetic mean of the surface profile. SEM was used to visualize micro- and macrosurface features.

Statistical analysis

Scaffold groups (aligned and random fiber orientation) were analyzed for significant differences for biochemical analysis and mechanical response to compression ($n=4$ /group/time point). Tensile and shear testing were performed using different fiber orientations: both aligned fibers (parallel and perpendicular to the loading direction) and random fiber samples ($n=5$ /group/time point) were analyzed. Numerical and graphical results are displayed as mean \pm standard deviation. Significance was determined by using ANOVA and accepted at a p -value < 0.05 .

Results

Chondrocyte–scaffold interaction

Fiber scaffolds of varying fiber alignment were produced (Fig. 1). Chondrocytes seeded on electrospun scaffolds adopted varying morphologies based on the scaffold type. The microstructure orientation of the underlying matrix directed chondrocytes into an elongated morphology for cells grown on aligned scaffolds and rounder, polygonal morphology for cells grown on randomly oriented scaffolds (Fig. 1). After 4 weeks of culture, immunohistochemical staining revealed an intense type II collagen matrix with minimal staining for type I collagen (Fig. 1).

Chondrocyte-seeded aligned and randomly oriented scaffolds exhibited significant increases in the sGAG content with no significant changes in DNA amount after 4 weeks in culture (p -value < 0.05) (Fig. 2). The sGAG amount was not statistically different between the scaffold groups $663 \pm 103 \mu\text{g}$ on randomly oriented versus $474 \pm 130 \mu\text{g}$ for the aligned scaffolds (p -value > 0.05).

Mechanical properties

Tensile and compressive properties of the scaffolds were determined after 4 weeks *in vitro* culture (Table 1). As expected, tensile properties were dependent on fiber orientation with the aligned fiber scaffolds having the highest tensile modulus. Tensile tests were performed for the duration of the culture period and showed no significant changes between acellular and cellular groups for either the aligned or random scaffold groups (Table 1). Compressive testing demonstrated a significant reduction in the compressive modulus of cellular scaffolds for both aligned and random fiber orientation after 4 weeks *in vitro* culture (Table 1). The cellular scaffolds showed a significantly lower compressive Young's modulus compared to articular cartilage, which according to previous studies, is of the order of $\sim 0.5 \text{ MPa}$

(bovine).^{35,36} Due to the differences in mechanical properties, scaffolds underwent different compressive strains, and these equivalent strains were calculated for the compressive shear testing loads of 0.04 and 0.08 MPa. These loads ranged from 16–31% strain (Table 2), which were in the physiological range of articular cartilage. Stress relaxation tests of 2% and 18% axial compressive strain were performed on cellular and acellular scaffolds to verify the presence of interstitial fluid support represented by the stress relaxation response (Table 3).

Shear testing

Shear testing was performed on cellular and acellular scaffolds (as well as on native articular cartilage) to assess frictional properties at two different loads corresponding to two different axial strains (Table 2). The equilibrium friction coefficient (μ_{eq}) was recorded at the end of the test (3600 s) to compare between cellular, acellular, and varying fiber orientation (Table 1). The mechanical shear tests were performed according to three different fiber directions. For the aligned anisotropic fiber scaffolds, the scaffolds were sheared in the parallel orientation to the fiber scaffold (in the fiber direction) or transverse or perpendicular fiber orientation (90° respective to the primary fiber orientation). Randomly oriented fiber scaffolds were also tested.

Representative shear curves for each scaffold type, fiber orientation, and loading condition are shown for acellular and cellular scaffolds in Figures 3 and 4. The frictional response of native articular cartilage when subjected to the same sliding test conditions at 0.04 and 0.08 MPa is also shown in Figures 4a and b. In addition, a further test using a normal load (i.e., a compressive load perpendicular to the surface) of 30N, which corresponds to an average contact pressure of 0.4 MPa, was performed to confirm the trend between the equilibrium friction coefficient and load. The effect of the increased contact pressure on the friction

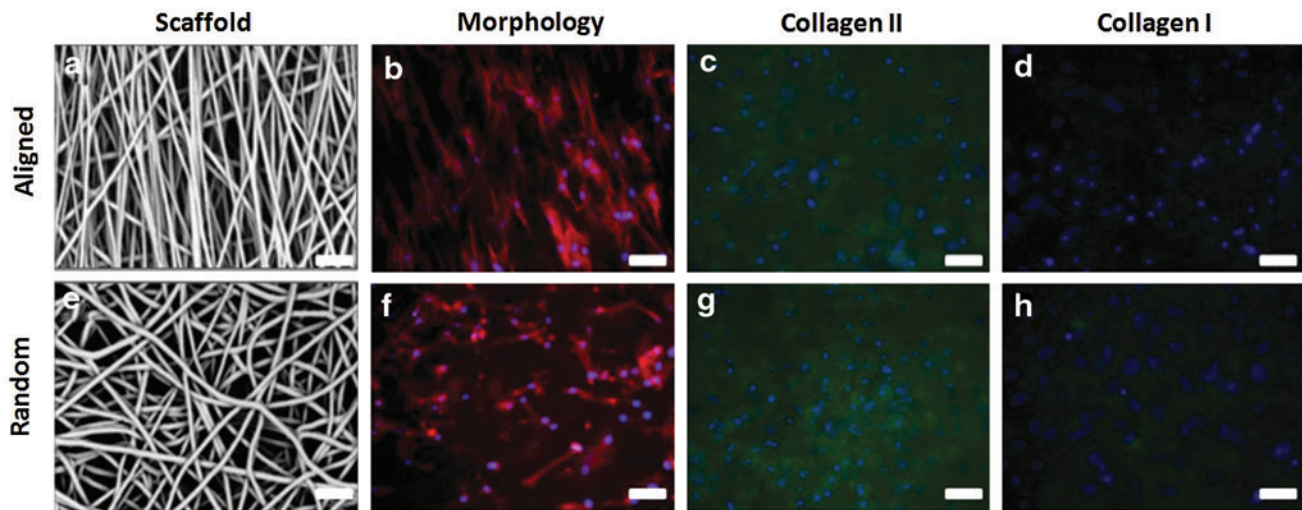


FIG. 1. Scaffold and chondrocyte morphology on aligned (a–d) and random (e–h) fiber scaffolds. Chondrocyte morphology was dramatically affected by fiber orientation (b, f). Immunohistochemical staining revealed intense staining for type II collagen matrix (c, g) with minimal type I collagen staining (d, h). Actin cytoskeleton = red; type I/II collagen = green, cell nuclei = blue; scale bar = 20 μm . Color images available online at www.liebertpub.com/tea

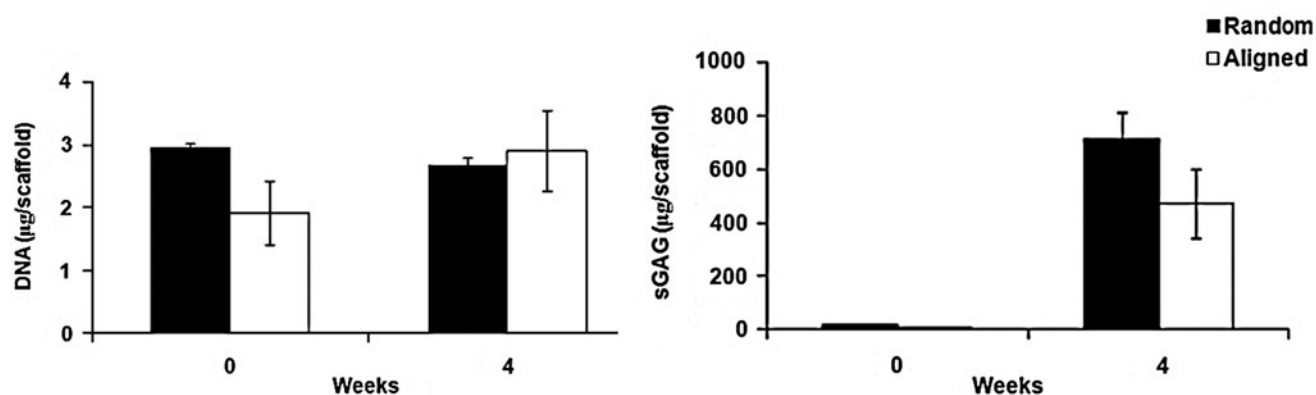


FIG. 2. Chondrocyte-seeded scaffolds did not exhibit any significant differences in DNA content following 4 weeks of culture, while significant increases were noted for sulfated glycosaminoglycans (sGAG) for both random and aligned scaffolds (p -value < 0.05). sGAG content was not significantly different between the scaffold groups after 4 weeks *in vitro* culture.

coefficient of articular cartilage was also verified (Supplementary Fig. S1; Supplementary Data are available online at www.liebertpub.com/tea).

According to the results, fiber orientation of the scaffolds seems to only slightly affect μ_{eq} , although the overall trend of the frictional response remains unchanged (Fig. 4a, b). At 0.04 MPa, for the cellular scaffolds, there is no statistically significant difference in μ_{eq} between random, parallel, and perpendicular fiber orientation, while the acellular scaffolds display differences based on fiber orientation (Fig. 4a). The random orientation acellular scaffolds exhibit the highest friction with $\mu_{eq} 0.96 \pm 0.11$, while the perpendicular alignment had the lowest friction with $\mu_{eq} 0.72 \pm 0.12$ (0.04 MPa) (Table 1). At 0.08 MPa, acellular scaffolds display almost identical μ_{eq} (Fig. 4b); possibly due to the higher normal load producing a similar surface morphology for all scaffold orientations.

The frictional response for the cellular scaffolds is very similar at both loads (Fig. 4a, b) with the perpendicular construct displaying a statistically significant higher friction coefficient compared to the other orientations at 0.08 MPa (Table 1). The addition of the ECM on the scaffold surfaces does not affect the trend in the frictional response although it does increase μ_{eq} .

Surface properties and damage assessment

Surface images of native (before undergoing shear testing), acellular, and cellular scaffolds of random and aligned

fiber configuration were recorded before and after shear testing using SEM and WLI. Before shear testing and cell culture, random acellular scaffolds were found to have a significantly lower mean surface roughness compared to the acellular aligned scaffolds (p -value < 0.05) (Table 4). With the cell-based deposition of the ECM, the fiber network became distorted and was less visible, homogenizing the surface, and yielding a very similar surface roughness between cellular random and cellular aligned scaffolds (Fig. 5 and Table 4). For the cellular scaffolds, following a 1-h shear test (corresponding to 7200 sliding cycles), WLI revealed surface disruption of the ECM and the fiber architecture underlying the deposited ECM (Fig. 6a, b). Significant surface disruption to the acellular scaffolds following shear is clearly visible at both loading regimes (Fig. 6a, b). A decrease in the mean surface roughness value, R_a , occurred following shear testing (Table 4) for all fiber orientations and at both loads. A statistically higher surface roughness of the cellular perpendicular tested scaffolds at 0.08 MPa was found compared to the other orientations indicating a higher surface damage (p -value < 0.05). The surface topography of articular cartilage was also assessed using WLI to provide a comparison for the tissue-engineered scaffolds (Supplementary Fig. S1). The surface roughness of articular cartilage was in agreement with our previously published work.³² Contrary to the scaffolds, the surface roughness following shear testing was seen to increase as previously reported in.³² SEM of the scaffold

TABLE 1. TENSILE AND COMPRESSIVE MODULUS OF CELLULAR AND ACELLULAR SCAFFOLDS

Mechanical parameter	Acellular			Cellular		
	Aligned parallel	Aligned perpendicular	Random	Aligned parallel	Aligned perpendicular	Random
Tensile Young's modulus (MPa)	28.07 ± 1.59	1.84 ± 0.08	8.15 ± 0.95	20.22 ± 5.30	2.11 ± 0.29	8.43 ± 0.30
Compressive Young's modulus (kPa)	179.00 ± 7.00		162 ± 33.30	100 ± 14.60 ^a		139.66 ± 5.30 ^a
Equilibrium friction coefficient at 0.04 MPa (μ_{eq})	0.78 ± 0.12	0.72 ± 0.12	0.96 ± 0.11	1.14 ± 0.16	1.10 ± 0.09	1.25 ± 0.09
Equilibrium friction coefficient at 0.08 MPa (μ_{eq})	0.48 ± 0.06	0.41 ± 0.05	0.44 ± 0.05	0.80 ± 0.09	0.87 ± 0.1 ^a	0.69 ± 0.08

^aDenotes statistically significant difference in compressive modulus between acellular and cellular samples and equilibrium friction coefficient between varying fiber orientations (p -value < 0.05).

TABLE 2. AXIAL STRAIN ON SCAFFOLDS AT 3N AND 6N (0.04 AND 0.08 MPa, RESPECTIVELY), COMPRESSIVE LOAD

Strain (MPa)	Acellular		Cellular	
	Aligned	Random	Aligned	Random
0.04	0.16 ± 0.01	0.17 ± 0.01	0.22 ± 0.02	0.18 ± 0.01
0.08	0.24 ± 0.01	0.26 ± 0.01	0.31 ± 0.02	0.27 ± 0.01

surface after shear testing confirmed the removal and formation of rolls of the ECM (Fig. 6a, b).

Discussion

We fabricated fibrous scaffolds of varying fiber orientation of either aligned or randomly oriented matrices to evaluate the effect of scaffold fiber orientation and its effect on the frictional response of tissue-engineered cartilage. Tensile properties of the engineered tissues varied significantly depending upon the fiber orientation, but were maintained after a short-term (4-week) culture duration (Table 1). With the addition of the cell-deposited ECM to the fibrous scaffolds, the compressive properties changed significantly, with the compressive modulus decreasing by 44% (Table 1). Thus, the axial strain on the scaffolds at loads of either 0.04 or 0.08 MPa varied between 16% and 31% (Table 2). This range of values represents the physiological strain, which articular cartilage is subjected to in the natural joint.^{37,38}

Under low-compressive strains, relaxation in the acellular scaffold diminished, indicating little fluid load support due to the high permeability of the scaffold construct. Stress relaxation was significantly higher for the cellular scaffolds, contributing to higher interstitial fluid pressurization and a stress relaxation response more similar to articular cartilage³⁹ (Table 3). At higher compressive strains such as 18%, the mechanical responses were dictated by the properties of the substrate, in this case, the scaffold itself, which offers no or

TABLE 3. STRESS RELAXATION OF CELLULAR AND ACELLULAR SCAFFOLDS AT 1 AND 5 MIN FOLLOWING 2% AND 18% APPLIED AXIAL STRAIN

Stress relaxation	2% axial strain			
	Acellular		Cellular	
	Random	Aligned	Random	Aligned
After 1 min (%)	3.94 ± 0.41	7.32 ± 0.29	5.58 ± 0.73	7.30 ± 0.47
After 5 min (%)	9.53 ± 3.47	12.97 ± 1.49	13.78 ± 0.19 ^a	19.05 ± 3.64 ^a
Stress relaxation	18% axial strain			
	Acellular		Cellular	
	Random	Aligned	Random	Aligned
After 1 min (%)	6.32 ± 1.48	8.27 ± 0.22	5.37 ± 2.50	7.78 ± 0.71
After 5 min (%)	10.93 ± 1.35	13.30 ± 1.21	9.87 ± 0.18	14.34 ± 2.43

^aDenotes statistically significant difference between stress relaxation rate of acellular and cellular samples at 2% applied axial compressive strain.

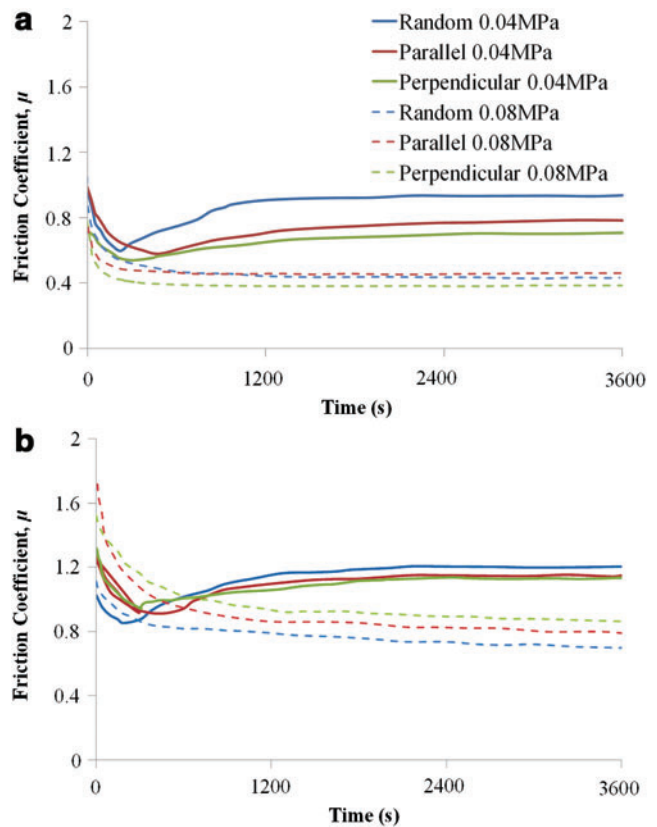


FIG. 3. Representative frictional response of (a) acellular (acell) and (b) cellular (cell) scaffolds at varying fiber orientation and varying contact pressure. Color images available online at www.liebertpub.com/tea

very limited interstitial fluid pressurization, and hence, fluid support, explaining the similarity in stress relaxation between cellular and acellular samples in Table 3.

The characteristic time-dependent frictional response of articular cartilage under shear testing is shown in Supplementary Figure S1 for three different loads. The frictional changes due to shear reflect the different lubrication mechanisms associated with articular cartilage. Initially, the friction coefficient is low (typically < 0.15) and is due to the fluid pressurization mechanism,⁴⁰ which generates a fluid film separating the surfaces. As shearing progresses, the fluid is expelled from the contact zone and the increased friction is due to the increased solid–solid interaction.

The frictional response of acellular and cellular scaffolds is very different to articular cartilage and is indicative that the underlying lubrication mechanisms are different. Low-friction coefficients at the start of the test are not observed for the tissue-engineered articular cartilage, which suggests that the fluid pressurization mechanism present in the cellular scaffold is absent. The frictional responses at both 0.04 MPa and 0.08 MPa show similar trends regardless of the cellular presence and fiber orientations (Fig. 4). The presence of the ECM on the surface as well as the orientation of the fibers appear to govern the equilibrium friction coefficient, while not affecting the overall trend. The response of the scaffolds at 0.04 MPa can generally be described by an initial peak in friction coefficient followed by a transitional stage until an equilibrium friction coefficient is reached. The peak in

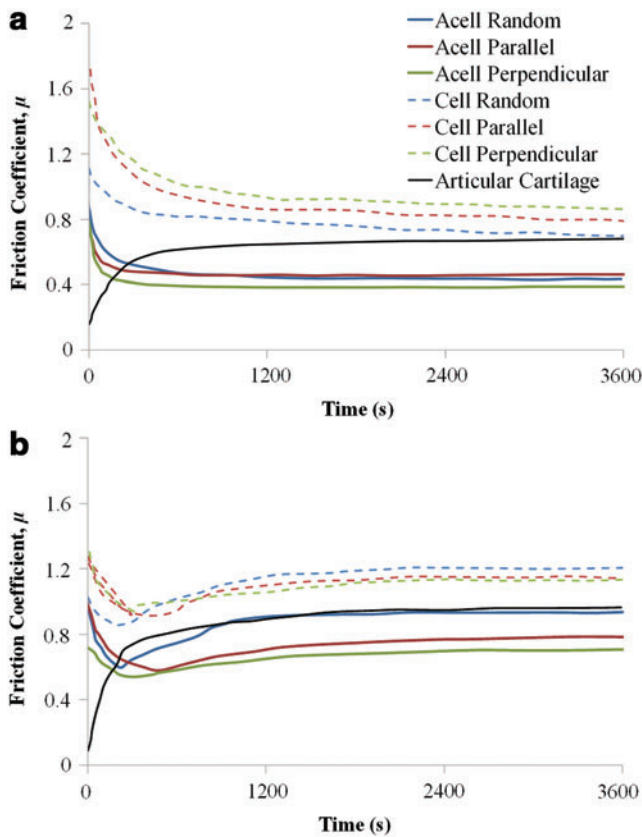


FIG. 4. Representative frictional response of acellular (acell) and cellular (cell) scaffolds at a contact pressure of (a) 0.04 MPa and (b) 0.08 MPa. Color images available online at www.liebertpub.com/tea

friction at the beginning of the test is due to the high surface roughness of the native scaffolds. The friction coefficient, following the initial peak, quickly decreases to a minimum value as some form of running in effect occurs. As the lubricating regime was predicted to be boundary, according to the analytical model used, the frictional response is particu-

TABLE 4. SURFACE PARAMETERS OF ARTICULAR CARTILAGE AND SCAFFOLDS UNDER NATIVE CONDITIONS AND AFTER 1 H OF SHEAR TESTING AT CONTACT PRESSURES OF 0.04 AND 0.08 MPa

Material	Surface parameters		
	Native R_a (μm)	0.04 MPa R_a (μm)	0.08 MPa R_a (μm)
Articular cartilage	0.64 ± 0.11	0.79 ± 0.17	1.15 ± 0.38
Acell-parallel	5.09 ± 0.83	2.82 ± 0.51	2.67 ± 0.95
Acell-perpendicular		2.76 ± 0.95	1.75 ± 0.81
Acell-random	3.29 ± 0.49^a	3.41 ± 0.56	1.81 ± 0.27
Cell-parallel	3.86 ± 1.05	3.33 ± 0.84	1.94 ± 0.40
Cell-perpendicular		3.71 ± 0.98	3.57 ± 1.18^a
Cell-random	3.26 ± 0.67	2.87 ± 0.49	2.08 ± 0.80

^aDenotes statistically significant difference in mean surface roughness between acellular and cellular samples or varying fiber orientations (p -value < 0.05). Acell and cell refer to acellular and cellular scaffolds, respectively.

larly susceptible to changes in surface roughness and topography. Once the minimum is reached, the friction coefficient increases and stabilizes to the equilibrium value, μ_{eq} , which is, however, lower than the start-up friction coefficient. The reason for the increase in the friction coefficient following the minimum can be explained by the formation of debris and surface damage on the scaffold as it occurs both for acellular and cellular specimens. At this contact pressure (0.04 MPa), it is likely that after the initial running in, the formation of surface features and debris plays a role in promoting a subsequent increase of the surface roughness as the surface pressure is probably not sufficient to flatten them. This is supported by the fact that the final surface roughness of the specimens tested at this load is generally higher than the roughness measured for the specimens after testing at 0.08 MPa.

The WLI images show significant disruption to the fiber network on the surface of the scaffolds following shear testing (Fig. 6a, b). Application of the load creates a more homogenous surface and a reduced surface roughness (R_a) as compared to the native scaffolds (Table 4). At 0.08 MPa load, following the peak in friction coefficient at the beginning of the test, a gradual decrease in friction occurs until an equilibrium value is reached. The transitional stage is absent at the 0.08 MPa load. This could be explained by the WLI results (Table 4), which show a significantly lower surface roughness after shear testing as compared to the native scaffolds and, as previously suggested, to the scaffolds subjected to the 0.04 MPa load shear test. The final smoother surface, due to the higher compressive load, causes the equilibrium coefficient to stabilize at a lower value with respect to the 0.04 MPa load case.

SEM images (Fig. 6), show extensive surface damage on the scaffolds following shear testing. As suggested in previous studies, scaffold debris released during sliding could potentially be acting as a boundary lubricant lowering μ_{eq} with increasing load.¹⁷ Overall, the surface roughness is higher for the cellular case based on (1) the ECM being removed with shear and rolling over itself across the surface in the direction parallel to sliding restricting the motion and increasing μ_{eq} and (2) the adhesion mechanisms that occur in articular cartilage.⁴¹ Adhesion is associated with an increase in friction,⁴² especially after long compression times caused by the increased effect of adhesive asperity microcontacts.⁴¹

The tissue-engineered scaffolds did not demonstrate the time-dependent frictional response typical of articular cartilage (Supplementary Fig. S1). The cell-deposited ECM layer is limited in thickness ($\sim 50 \mu\text{m}$), as determined by histological staining in some of the authors' previous work,¹⁵ and due to the scaffolds being under significant axial strain, the frictional response is dominated by the scaffold (Table 2). Although the scaffold itself is biphasic, as it is constituted by a solid phase of tightly nonwoven fibers hydrated by a fluid phase consisting of water, it is thought that its permeability is too high to allow any interstitial fluid pressure to form as the fluid is easily exuded out of the material, as shown by the stress relaxation values in Table 2. At high strains, 16%–31% (Table 2), equivalent to conditions experienced during sliding, the stress relaxation was low due to the minor contribution of the cell-deposited ECM and the low fluid support of the scaffold. This agrees with the hypothesis that the sliding tests showed no sign of interstitial fluid pressurization. Other studies^{10,16,19} have reported interstitial

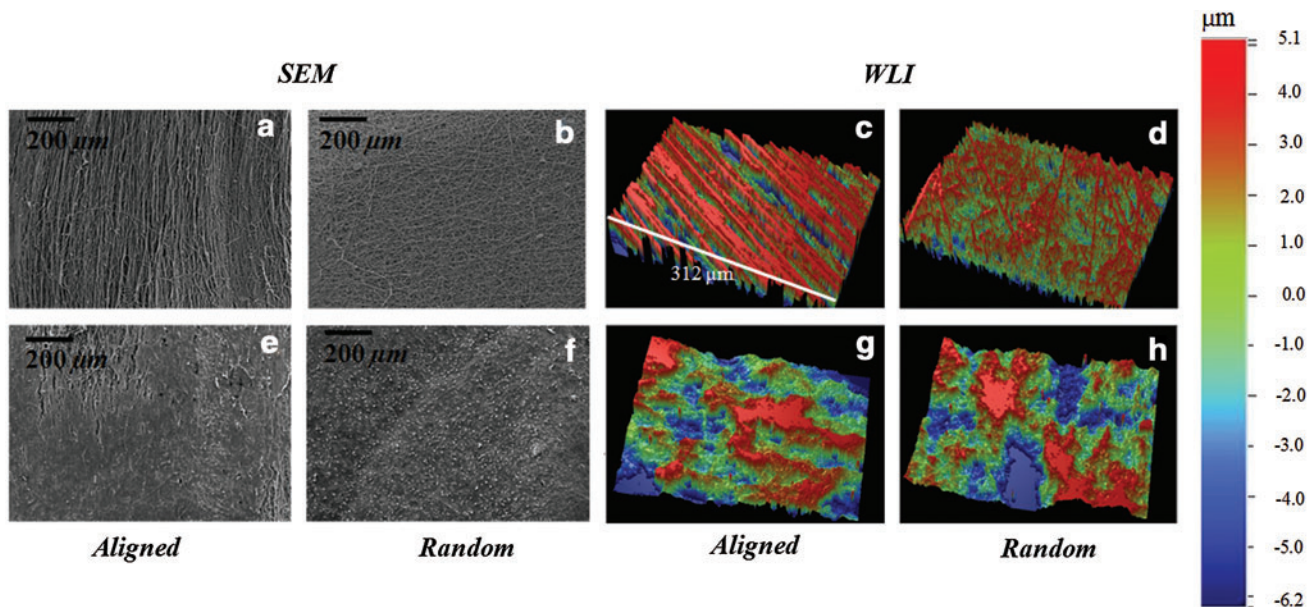


FIG. 5. Scanning electron microscopy (SEM) and white light interferometry (WLI) images of native acellular and cellular scaffolds in aligned (a, e, c, g) and random (b, f, d, h) configurations. After 4 weeks *in vitro* (e, f, g, h), the fiber networks became distorted due to extracellular matrix deposition (variances in matrix deposition were noted). SEM, scanning electron microscopy; WLI, white light interferometry. Color images available online at www.liebertpub.com/tea

pressurization in tissue-engineered scaffolds. These, however, were very different material constructs and/or were subjected to extremely small normal loads and applied strains. Under these conditions, the frictional response was solely or mostly given by the response of the ECM rather than the scaffold.^{10,16,19} Previous studies have shown a higher equilibrium friction coefficient for tissue-engineered articular cartilage,^{10,16} while others have shown a lower μ_{eq} compared to native articular cartilage.^{17,19} These variances can be based on testing conditions/configurations, the type of scaffold used, and cell culture duration/conditions, including the type of cell.¹⁸

No significantly relevant differences in μ_{eq} between fiber orientations were found for the cellular scaffolds. Minor variations between fiber orientations can be attributed to differences in the evolution of surface damage as a result of shearing. For the cellular scaffold sheared at 0.08 MPa, the perpendicular orientation exhibited a statistically higher friction compared to the random and parallel orientation. The high μ_{eq} for the perpendicular scaffold could be due to the excessive damage occurring as a result of sliding and is supported by the WLI measurements (Table 4), which indicate a significantly higher surface roughness for the perpendicular samples following sliding compared to the other orientations at 0.08 MPa. This supports the notion that surface roughness plays a dominating role in the frictional response. SEM images of the perpendicular scaffold show more disrupted fibers on the surface as compared to the other two orientations.

For the acellular case, a more prominent difference in the frictional response according to fiber orientation was found compared to the cellular scaffolds; at 0.04 MPa, the random fiber orientation exhibited the highest equilibrium friction coefficient, while the perpendicular, the lowest. This agrees with the surface roughness of the acellular scaffolds follow-

ing sliding obtained using WLI; the random orientation has, overall, a rougher surface compared to the perpendicular case (Table 1). In this study, the surface roughness and damage appear to be the main governing factors of μ_{eq} . The onset of damage on the scaffold's surface is thought to be dictated by the orientation of the fiber network. We hypothesize that for the cellular case, the cell-deposited ECM layer masks the fiber homogenization effect occurring at the surface, and hence, the frictional response of the cellular scaffolds compared to acellular at 0.04 MPa.

At 0.08 MPa for the acellular scaffolds, the almost identical μ_{eq} across the different fiber orientations has been attributed to the similar surface morphology of the scaffolds following shear. This is confirmed by the WLI images in Figure 6, where the fiber network appears completely homogenized after shear. Only the parallel orientation seems to have some fibers still intact on the surface, probably due to superior mechanical properties when subject to tension, along the fiber direction. The parallel fiber sample following shear has a higher R_a compared to the two other orientations, and this is probably due to the fibers, which are still present on the surface. It should be highlighted that the frictional response of the engineered tissues is the result of the interplay between substrate morphology, surface evolution, fluid/solid interactions, and applied load.

In summary, the frictional response of the engineered tissues was not influenced by the fiber orientation. This suggests that when inserting the scaffolds in the joint, the choice of fiber orientation is not particularly important in terms of the frictional response, but it is, however, fundamental with regard to damage resistance and resistance to tension arising from shearing. Collagen damage is, in fact, thought to originate from excessive shear and strain along the fiber direction.⁴³ Hence, when inserted into the joint, either the aligned scaffolds should be oriented along

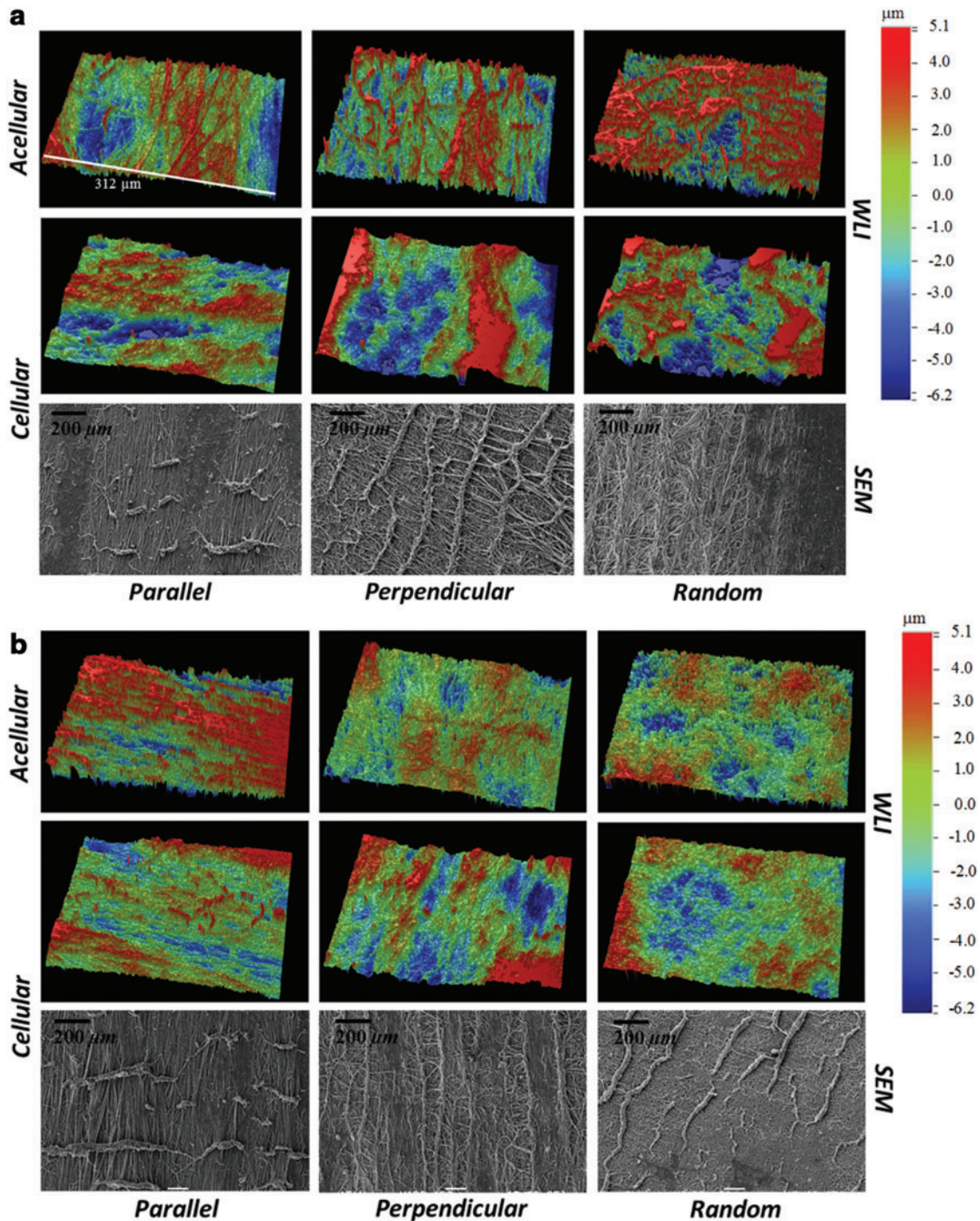


FIG. 6. Surface topography images using WLI and SEM following a 1-h shear test with a normal load of (a) 0.04 MPa and (b) 0.08 MPa. Color images available online at www.liebertpub.com/tea

the direction of shear and motion or the random scaffold orientation should be implanted. Although the random fiber orientation provides significantly lower tensile properties, it yields a better topographical surface for friction and wear based on the isotropic orientation of the matrix. With this in mind, it is thought that the collagen fibers in the superficial zone are oriented in the direction of maximum tensile strain.⁴⁴ Furthermore, this study suggests that for tissue-engineered articular cartilage to mimic the mechanical and

frictional response of articular cartilage at physiological strains, the cell culture time should be long enough to allow a full-thickness ECM, and hence, articular cartilage to form. This would allow the scaffold-articular cartilage construct to better resist in-joint physiological stresses and strains prolonging the life of the scaffold in the joint that is essential in providing the foundation for the proliferation of chondrocytes, and hence, the successful formation of native articular cartilage.

Conclusions

In conclusion, the results obtained from this study suggest that aligned microfibrillar scaffolds provide improved surfaces for superficial zone tissue engineering of articular cartilage, as compared to random fiber networks and could offer a potentially promising solution for the treatment of articular cartilage defects and localized early OA. However, studies involving longer culture times to allow full-thickness ECM growth on the scaffold surface should be envisaged to allow a more direct comparison to articular cartilage and, thus, to better evaluate the true clinical potential of such a technique. Future studies should also test different scaffold materials and varying fiber sizes to establish the effect of such variations on the frictional response.

Acknowledgments

M.A. Accardi, P.M. Cann, and D. Dini acknowledge the financial support of the Taiho Kogyo Tribology Research Foundation. M.A. Accardi thanks the EPSRC and the Department of Mechanical Engineering for the financial support via a Doctoral Training Award. M.M. Stevens and S.D. McCullen thank the Medical Engineering Solutions in Osteoarthritis Centre of Excellence funded by the Wellcome Trust and the EPSRC for funding. A. Callanan thanks the Irish Research Council for Science, Engineering and Technology (IRCSET) – Marie Curie International Mobility Fellowship co-funded grant PD/2010/INSP/1948 for funding.

Disclosure Statement

No competing financial interests exist.

References

1. Meachim, G. Effect of age on the thickness of adult articular cartilage at the shoulder joint. *Ann Rheum Dis* **30**, 43, 1971.
2. Buckwalter, J.A., and Martin, J.A. Osteoarthritis. *Adv Drug Deliv Rev* **58**, 150, 2006.
3. Brittberg, M. Cell carriers as the next generation of cell therapy for cartilage repair: a review of the matrix-induced autologous chondrocyte implantation procedure. *Am J Sports Med* **38**, 1259, 2010.
4. Nuernberger, S., Cyran, N., Albrecht, C., Redl, H., Vecsei, V., and Marlovits, S. The influence of scaffold architecture on chondrocyte distribution and behavior in matrix-associated chondrocyte transplantation grafts. *Biomaterials* **32**, 1032, 2011.
5. Behrens, P., Ehlers, E.M., Kochermann, K.U., Rohwedel, J., Russlies, M., and Plotz, W. New therapy procedure for localized cartilage defects. Encouraging results with autologous chondrocyte implantation. *MMW Fortschr Med* **141**, 49, 1999.
6. Basad, E., Ishaque, B., Bachmann, G., Sturz, H., and Steinmeyer, J. Matrix-induced autologous chondrocyte implantation versus microfracture in the treatment of cartilage defects of the knee: a 2-year randomised study. *Knee Surg Sports Traumatol Arthrosc* **18**, 519, 2010.
7. Erggelet, C., Kreuz, P.C., Mrosek, E.H., Schagemann, J.C., Lahm, A., Ducommun, P.P., *et al.* Autologous chondrocyte implantation versus ACI using 3D-bioresorbable graft for the treatment of large full-thickness cartilage lesions of the knee. *Arch Orthop Trauma Surg* **130**, 957, 2010.
8. Albrecht, C., Tichy, B., Nurnberger, S., Hosiner, S., Zak, L., Aldrian, S., *et al.* Gene expression and cell differentiation in matrix-associated chondrocyte transplantation grafts: a comparative study. *Osteoarthritis Cartilage* **19**, 1219, 2011.
9. Harris, J.D., Siston, R.A., Brophy, R.H., Lattermann, C., Carey, J.L., and Flanigan, D.C. Failures, re-operations, and complications after autologous chondrocyte implantation—a systematic review. *Osteoarthritis Cartilage* **19**, 779, 2011.
10. Morita, Y., Tomita, N., Aoki, H., Sonobe, M., Wakitani, S., Tamada, Y., *et al.* Frictional properties of regenerated cartilage *in vitro*. *J Biomech* **39**, 103, 2006.
11. Mager, M.D., LaPointe, V., and Stevens, M.M. Exploring and exploiting chemistry at the cell surface. *Nat Chem* **3**, 582, 2011.
12. Place, E.S., Evans, N.D., and Stevens, M.M. Complexity in biomaterials for tissue engineering. *Nat Mater* **8**, 457, 2009.
13. Baker, B.M., and Mauck, R.L. The effect of nanofiber alignment on the maturation of engineered meniscus constructs. *Biomaterials* **28**, 1967, 2007.
14. Wise, J.K., Yarin, A.L., Megaridis, C.M., and Cho, M. Chondrogenic differentiation of human mesenchymal stem cells on oriented nanofibrous scaffolds: engineering the superficial zone of articular cartilage. *Tissue Eng Part A* **15**, 913, 2009.
15. McCullen, S.D., Autefage, H., Callanan, A., Gentleman, E., and Stevens, M.M. Anisotropic fibrous scaffolds for articular cartilage regeneration. *Tissue Eng Part A* **18**, 2073, 2012.
16. Lima, E.G., Bang, L.M., Srerebrov, A., Mauck, R.T., Byers, B.A., Tuan, R., *et al.* Measuring the frictional properties of tissue-engineered cartilage constructs. *Proceedings of the 52nd Orthopaedic Research Society, Chicago, IL*, 2006.
17. Plainfosse, M., Hatton, P.V., Crawford, A., Jin, Z.M., and Fisher, J. Influence of the extracellular matrix on the frictional properties of tissue-engineered cartilage. *Biochem Soc Trans* **35**, 677, 2007.
18. Moutos, F.T., and Guilak, F. Functional properties of cell-seeded three-dimensionally woven poly(epsilon-caprolactone) scaffolds for cartilage tissue engineering. *Tissue Eng Part A* **16**, 1291, 2010.
19. Gleghorn, J.P., Jones, A.R., Flannery, C.R., and Bonassar, L.J. Boundary mode frictional properties of engineered cartilaginous tissues. *Eur Cell Mater* **14**, 20; discussion 8, 2007.
20. Nerurkar, N.L., Han, W.J., Mauck, R.L., and Elliott, D.M. Homologous structure-function relationships between native fibrocartilage and tissue engineered from MSC-seeded nanofibrous scaffolds. *Biomaterials* **32**, 461, 2011.
21. Klein, T.J., Malda, J., Sah, R.L., and Huttmacher, D.W. Tissue engineering of articular cartilage with biomimetic zones. *Tissue Eng Part B Rev* **15**, 143, 2009.
22. Li, W.J., Cooper, J.A., Mauck, R.L., and Tuan, R.S. Fabrication and characterization of six electrospun poly(alpha-hydroxy ester)-based fibrous scaffolds for tissue engineering applications. *Acta Biomater* **2**, 377, 2006.
23. Chew, S.Y., Wen, Y., Dzenis, Y., and Leong, K.W. The role of electrospinning in the emerging field of nanomedicine. *Curr Pharm Des* **12**, 4751, 2006.
24. Shao, Z., Zhang, X., Pi, Y., Wang, X., Jia, Z., Zhu, J., *et al.* Polycaprolactone electrospun mesh conjugated with an MSC affinity peptide for MSC homing *in vivo*. *Biomaterials* **33**, 3375, 2012.
25. Nerurkar, N.L., Elliott, D.M., and Mauck, R.L. Mechanics of oriented electrospun nanofibrous scaffolds for annulus fibrosus tissue engineering. *J Orthop Res* **25**, 1018, 2007.
26. Ayres, C.E., Jha, B.S., Meredith, H., Bowman, J.R., Bowlin, G.L., Henderson, S.C., *et al.* Measuring fiber alignment in

- electrospun scaffolds: a user's guide to the 2D fast Fourier transform approach. *J Biomater Sci Polym Ed* **19**, 603, 2008.
27. Newton, D., Mahajan, R., Ayres, C., Bowman, J.R., Bowlin, G.L., and Simpson, D.G. Regulation of material properties in electrospun scaffolds: Role of cross-linking and fiber tertiary structure. *Acta Biomater* **5**, 518, 2009.
 28. Girard, M.J., Dahlmann-Noor, A., Rayapureddi, S., Bechara, J.A., Bertin, B.M., Jones, H., *et al.* Quantitative mapping of scleral fiber orientation in normal rat eyes. *Invest Ophthalmol Vis Sci* **52**, 9684, 2011.
 29. Scaraggi, M., Carbone, G., Persson, B.N.J., and Dini, D. Lubrication in soft rough contacts: a novel homogenized approach. Part I—theory. *Soft Matter* **7**, 10395, 2011.
 30. Scaraggi, M., Carbone, G., and Dini, D. Lubrication in soft rough contacts: a novel homogenized approach. Part II - Discussion. *Soft Matter* **7**, 10407, 2011.
 31. Persson, B.N.J., and Scaraggi, M. On the transition from boundary lubrication to hydrodynamic lubrication in soft contacts. *J Phys Condensed Matter* **21**, 185002, 2009.
 32. Accardi, M.A., Cann, P.M., and Dini, D. Experimental and numerical investigation of the behaviour of articular cartilage under shear loading—interstitial fluid pressurisation and lubrication mechanisms. *Tribology Int* **44**, 565, 2011.
 33. Graindorger, S., Ferrandez, W., Fisher, J., Grant, C., Ingham, E., Twigg, P., *et al.* Biphasic surface amorphous layer lubrication of articular cartilage. *Med Eng Phys* **27**, 836, 2005.
 34. Shekhawat, V.K., Laurent, M., Muehleman, C., and Wimmer, M.A. Characterizing the Surface Topography of Viable Cartilage Explants—A Novel Application of the Scanning White Light Interferometer. Proceedings of the ASME Summer Bioengineering Conference, Marco Island, FL, 2008.
 35. Jurvelin, J.S., Kiviranta, P., Rieppo, J., Korhonen, R.K., Julkunen, P., and Toyras, J. Collagen network primarily controls Poisson's ratio of bovine articular cartilage in compression. *J Orthop Res* **24**, 690, 2006.
 36. Jurvelin, J.S., Buschmann, M.D., and Hunziker, E.B. Mechanical anisotropy of the human knee articular cartilage in compression. *Proc Inst Mech Eng H* **217**, 215, 2003.
 37. Bingham, J.T., Papannagari, R., de Velde, S.K.V., Gross, C., Gill, T.J., Felson, D.T., *et al.* *In vivo* cartilage contact deformation in the healthy human tibiofemoral joint. *Rheumatology* **47**, 1622, 2008.
 38. Yang, N.H., Nayeb-Hashemi, H., Canavan, P.K., and Vaziri, A. Effect of frontal plane tibiofemoral angle on the stress and strain at the knee cartilage during the stance phase of gait. *J Orthop Res* **28**, 1539, 2010.
 39. Mow, V.C., Kuei, S.C., Lai, W.M., and Armstrong, C.G. Biphasic creep and stress relaxation of articular cartilage in compression: theory and experiments. *J Biomech Eng* **102**, 73, 1980.
 40. Ateshian, G. A Theoretical formulation for boundary friction in articular cartilage. *J Biomech Eng* **119**, 81, 1997.
 41. Chan, S.M.T., Neu, C.P., Komvopoulos, K., and Reddi, A.H. The role of lubricant entrapment at biological interfaces: reduction of friction and adhesion in articular cartilage. *J Biomech* **44**, 2015, 2011.
 42. Israelachvili, J., Chen, Y.L., Yoshizawa, H., Steinberg, S., Vigil, G., and Xu, Z.G. The relationship between adhesion and friction. *Vide Sci Tech Appl* **50**, 409, 1994.
 43. Wilson, W., van Burken, C., van Donkelaar, C., Buma, P., van Rietbergen, B., and Huiskes, R. Causes of mechanically induced collagen damage in articular cartilage. *J Orthop Res* **24**, 220, 2006.
 44. Fry, H.J. The interlocked stresses of articular cartilage. *Br J Plast Surg* **27**, 363, 1974.

Address correspondence to:

Daniele Dini, PhD

Tribology Group

Department of Mechanical Engineering

Imperial College London

London SW7 2AZ

United Kingdom

E-mail: d.dini@imperial.ac.uk

Molly M. Stevens, PhD

Departments of Materials, Bioengineering,

and Institute of Biomedical Engineering

Imperial College London

London SW7 2AZ

United Kingdom

E-mail: m.stevens@imperial.ac.uk

Received: September 25, 2012

Accepted: April 30, 2013

Online Publication Date: July 29, 2013